




Electrochemical Estimations of the Gold Nanoparticle Size Effect on Cysteine-Gold Oxidation

Elena Romanovskaia,^{1,2,*} Peter Slovenský,^{3,*} S. Marzieh Kalantarian,^{4,*} Lila Laundry-Mottiar,⁴ Valentin Romanovski,^{2,5} Maroš Halama,³ Michael Auinger,^{6,7,**} and Yolanda S. Hedberg^{1,4,8,**,z} 

¹KTH Royal Institute of Technology, School of Engineering Sciences in Chemistry, Biotechnology and Health, Department of Chemistry, Division of Surface and Corrosion Science, SE-10044 Stockholm, Sweden

²Department of Materials Science and Engineering, University of Virginia, Charlottesville, Virginia 22904, United States of America

³Technical University of Kosice, Faculty of Materials, Metallurgy and Recycling, Institute of Materials, 042 00 Košice, Slovakia

⁴Department of Chemistry, The University of Western Ontario, London, Ontario N6A 5B7, Canada

⁵Science and Research Centre of Functional Nano-Ceramics, National University of Science and Technology "MISIS," 119049 Moscow, Russia

⁶Institute of Chemical Technologies and Analytics, Technische Universität Wien, 1040 Vienna, Austria

⁷WMG, University of Warwick, Coventry CV4 7AL, United Kingdom

⁸Surface Science Western, The University of Western Ontario, London, Ontario N6G 0J3, Canada

Gold nanoparticles are interesting for nanobiomedical applications, such as for drug delivery and as diagnostic imaging contrast agents. However, their stability and reactivity in-vivo are influenced by their surface properties and size. Here, we investigate the electrochemical oxidation of differently sized citrate-coated gold nanoparticles in the presence and absence of L-cysteine, a thiol-containing amino acid with high binding affinity to gold. We found that smaller sized (5, 10 nm) gold nanoparticles were significantly more susceptible to electrochemical L-cysteine interactions and/or L-cysteine-facilitated gold oxidation than larger (20, 50 nm) sized gold nanoparticles, both for the same mass and nominal surface area, under the conditions investigated (pH 7.4, room temperature, stagnant solutions, and scan rates of 0.5 to 450 mV s⁻¹). The electrochemical measurements of drop-casted gold nanoparticle suspensions on paraffin-impregnated graphite electrodes were susceptible to the quality of the electrode. Increased cycling resulted in irreversible oxidation and detachment/oxidation of gold into solution. Our results suggest that L-cysteine-gold interactions are stronger for smaller nanoparticles.

© 2022 The Author(s). Published on behalf of The Electrochemical Society by IOP Publishing Limited. This is an open access article distributed under the terms of the Creative Commons Attribution 4.0 License (CC BY, <http://creativecommons.org/licenses/by/4.0/>), which permits unrestricted reuse of the work in any medium, provided the original work is properly cited. [DOI: 10.1149/1945-7111/ac4bf8]



Manuscript submitted October 21, 2021; revised manuscript received January 7, 2022. Published February 4, 2022. *This paper is part of the JES Focus Issue on Women in Electrochemistry.*

Gold (Au) nanoparticles (NPs) have been considered for a wide range of biomedical applications, following intravenous injection, because of their high density, relatively high chemical stability, and the possibility to attach agents such as tumor-targeting agents.^{1,2} The in-vivo environment, with its high ionic strength, high complexation capacity, and sometimes very oxidative environments is able to dissolve Au under certain conditions. While Au dissolution in-vivo has been called "unexpected" as late as 2020,³ it has been shown to occur, especially for oxidative environments containing biomolecules such as ligands or complexing agents and for small Au NPs, i.e. less than 10 nm in size in this study.^{4,5} independent of their coating (citrate or polyethylene glycol).⁵ Complexation-induced dissolution between Au and different ligands, including chlorides and amino acids, has been reported previously.^{6–8} Different oxidative environments, including Fenton reactants,⁴ triggered macrophages,⁴ and a peroxyxynitrite generator,⁵ were only able to increase Au dissolution from 5 nm Au NPs in the presence of other ligands, but not in pure water, sodium chloride, or from 20 or 50 nm Au NPs.

We found previously that citrate-coated 5 nm Au NPs reacted with L-cysteine and formed an Au thiolate complex, detected by means of time-of-flight secondary ion mass spectrometry.⁹ The interaction seemed to be stronger than for larger sized, 50 nm, Au NPs in the same study. Cyclic voltammetry (CV) in the same study⁹ revealed a stronger oxidation peak for the 5 nm Au NPs than for 50 nm Au NPs (for the same mass) and for higher L-cysteine

concentrations in the electrolyte. It was speculated⁹ whether there is a larger interaction between L-cysteine with 5 nm Au NPs, compared with larger nanoparticles, for the same surface area. CV in cysteine solutions using Au electrodes has been investigated in other studies as well, mainly focused on biosensing.^{10,11}

The aim of this study is to experimentally investigate any NP size effect for citrate-coated Au NPs, ranging from 5 to 50 nm in diameter, on their Au and/or amino acid oxidation peaks using CV. To be able to understand and interpret our data, we conducted these measurements in different control solutions, for equal mass and equal nominal surface area of NPs, for different scan rates and cycle numbers, and for different electrodes and potentiostats.

Experimental

Au NPs.—5, 10, 20, and 50 nm citrate-coated Au NP aqueous suspensions, stabilized in citrate buffer, were purchased from Sigma Aldrich, Sweden (article numbers 741949–25 ML, 741957–25 ML, 741965–25 ML, and 742007–25 ML). They were originally made in Canada. The suspensions were first investigated in Sweden (CV) and then shipped to Russia (for transmission electron microscopy—TEM), Slovakia (CV), and Canada (CV). They were stored refrigerated (4 °C) and vortexed prior to each pipetting. No color change or precipitation was visible throughout the study. The 5, 10, 20, and 50 nm Au NP suspensions, according to the supplier, contained 5.50 10¹³, 6.00 10¹², 6.54 10¹¹, and 3.5 10¹⁰ particles/ml, respectively.

For CV measurements comparing the same mass (0.56 μg) of nanoparticles, 8, 9.2, 10.5, and 12.6 μl of the suspensions of the 5, 10, 20, and 50 nm Au NPs, respectively, were pipetted onto a paraffin-impregnated graphite electrode (PIGE). For CV measurements comparing the same nominal surface area (0.086 cm²,

^zThese authors contributed equally to this work.

*Electrochemical Society Student Member.

**Electrochemical Society Member.

^zE-mail: yhedberg@uwo.ca

ignoring particle agglomeration), 2, 4.6, 10.5, and 31.4 μl of the 5, 10, 20, and 50 nm Au NP suspensions, respectively, were pipetted onto a PIGE.

For comparison, Au foil (0.1 mm thickness, 99.99% trace metal basis purity) was purchased from Sigma Millipore (article number 265810), Canada.

PIGE.—All PIGEs in this study were manufactured at Technical University of Košice, Slovakia, following the procedure specified by Scholz and Lange.¹² Graphite rods were immersed in molten paraffin (temperature 70 °C–80 °C) and kept under vacuum until no bubbles were evolving anymore (about 2–3 h), followed by removal of the graphite rods before the paraffin solidified. To manufacture the PIGEs of this work, different high-purity graphite rods were used. Also, the PIGEs used in this study might have contained different fractions of paraffin. Any resulting variability is discussed in the results and discussion section.

Chemicals.—The solvent for all experiments was ultrapure water (resistivity of 18.2 M Ωcm , Millipore Sigma, Canada and Sweden, and Rodem 6 Automat—Kusyn, Slovakia). L-cysteine (CAS 52–90–4, assay \geq 98%, product number C7352), L-lysine (CAS 56–87–1), and L-glutamic acid (CAS 56–86–0, Assaytra3) were purchased from Sigma Aldrich, Sweden, or Millipore Sigma, Canada. 2-(N-morpholino) ethane sulfonic acid (MES) buffer was obtained from Millipore Sigma (Canada and Sweden). Sodium chloride (analytical grade) and ultrapure nitric acid (67%) was obtained from VWR (Canada and Sweden). Sodium chloride (99.9% purity) was also obtained from ITES Vranov s.r.o., Slovakia. Dulbecco's modified Eagle medium (DMEM, GibcoArt. No. 41965-036) was purchased from Life Technologies (Thermo Fisher Scientific, USA), stored refrigerated (4 °C) and adjusted to pH 7.4 prior to use. Its full composition is given in Table A-1. Sodium dodecyl sulfate (99%, BPI66100), ethanol (99%), and acetone were purchased from Fisher Scientific, Canada.

TEM.—TEM measurements were conducted with a JEOL 2100 instrument (Jeol Ltd., Japan). The NP suspensions were dropped (diluted) from their suspension on the TEM grid, followed by drying. The IMAGEJ software (version 1.52 v) was used to quantitatively evaluate the size distribution of 196, 129, 208, and 114 individual particles for the 5, 10, 20, and 50 nm Au NPs, respectively. Data for the 5 nm Au NPs have been published previously,⁹ but is here included for comparison. The cumulative size distribution curves were plotted in Origin 2016 and differentiated. The resulting size distribution was smoothed using the adjacent-averaging method with ten points of window.

CV.—All measurements were conducted at least twice. The temperature in this study ranged from 22 to 25 °C. All measurements were conducted in aerated (not deaerated) conditions and in stagnant electrolytes, to avoid unnecessary detachment of Au NPs from the PIGE.

This study comprises CV measurements conducted by three different labs on the same Au NPs suspensions but using different potentiostats and PIGEs. We found some specific differences and they are discussed below. All labs used a small sized electrochemical cell (maximum capacity 5 ml), where the PIGE with or without any Au NPs was the working electrode, a platinum wire was the counter electrode, and a saturated calomel electrode, an Ag/AgCl sat. KCl electrode, or an Ag/AgCl 3 M KCl electrode was used as the reference electrode. All reference electrodes were checked against a master electrode prior to each measurement. In between measurements, they were also cleaned with 16 mM sodium dodecyl sulfate (SDS) to desorb any amino acids. To facilitate comparison, all data have been plotted against the saturated hydrogen electrode (SHE) in the following.

Potentiostat 1 was a PARSTAT MC Multichannel potentiostat (Princeton Applied Research) with a PMC-1000 channel.

Potentiostat 2 was a Solartron Analytical ModuLab potentiostat (1 MS/s DC channel), which was connected to isolated ground power via a Unified Power System, to minimize short power outage effects. Potentiostat 3 was an IviumStat (high power, general purpose potentiostat/galvanostat/ZRA).

All PIGE electrodes were freshly ground with 1200 SiC grit paper prior to each measurement, then cleaned with ultrapure water and ethanol. If Au NPs were investigated (all measurements except background control measurements), the appropriate volume (see section chemicals) of the corresponding suspension, after being vortexed for 10 s, was pipetted onto the PIGE and left to dry. When dried, the PIGE was inserted in the electrolyte for the measurement.

All electrolytes in this study were adjusted to a pH of 7.4 by NaOH or HNO₃, 5 g l⁻¹ NaCl was present in all electrolytes as well as 5 mM MES buffer. 0.5 mM L-cysteine was added for measurements in the presence of L-cysteine. For comparative amino acid measurements, 0.5 mM of the individual amino acid (L-cysteine, L-glutamic acid, and L-lysine) was present. DMEM was used as is, at pH 7.4.

All measurements started at open circuit potential, which was first determined for at least 5 min, and then scanned towards more positive potentials (1 or 1.5 V vs the reference electrode), followed by a negative scan to -1 or -1.5 V vs reference electrode and reversal to open circuit potential. The broader potential window of 1.5 to -1.5 V vs reference electrode was only selected for some higher scan rates. For selected measurements, up to 10 cycles were run. The scan rate varied between 0.5 and 450 mV s⁻¹ and is indicated in the figure captions.

The thin Au foil was cleaned with 16 mM SDS at 40 °C for 1 h, followed by rinsing with ultrapure water and 15 min ultrasonic cleaning in acetone, prior to each measurement. It was not (re) polished and the order of measurements was CV in 5 g l⁻¹ NaCl and 5 mM MES (pH 7.4, 25 °C) replicate 1 and 2, followed by 5 g l⁻¹ NaCl, 5 mM MES, and 0.5 mM L-cysteine (pH 7.4, 25 °C) replicate 1 and 2.

An overview on potentiostats, electrodes, and measurements of this study is given in Table A-II. Since the cyclic voltammograms presented in this study contain contributions both from the PIGEs and from the Au NPs, the current rather than a normalized current is shown. Either the mass or the nominal surface area of the Au NPs is held constant, as indicated in the figure captions.

Inductively coupled plasma mass spectrometry.—To investigate whether any Au was released into the electrolyte, either by detachment of Au NPs or by oxidation/dissolution of Au, the electrolyte solutions from 5 and of 50 nm Au NPs cycled for 10 cycles at 25 °C at 450 mV s⁻¹ in 5 g l⁻¹ NaCl, 5 mM MES, 0.5 mM L-cysteine, pH 7.4, were sampled for solution analysis. This CV was performed with Potentiostat 2 and PIGE 4. The solution was frozen (-20 °C) until digestion. For digestion, 3 ml of each solution were sampled and diluted four times with diluted aqua regia (final concentration of 0.07% HCl and 0.18% HNO₃) and digested using a Milestone ETHOD microwave digester. The temperature ramp settings were 170 °C over 10 min, then 10 min hold at 170 °C. A Thermo Scientific iCAP Q inductively coupled plasma mass spectrometer with no reaction gas was calibrated with 0, 10, 30, and 60 $\mu\text{g l}^{-1}$ Au (linear calibration curve, R² = 0.998). The instrument detection limit was 0.002 $\mu\text{g l}^{-1}$ Au. The uncertainty for a 30 $\mu\text{g l}^{-1}$ Au quality control standard was 7%, and blank samples (2% HNO₃) were below the detection limit. The percentage of released Au into solution was calculated by the measured concentration (2.2–6.0 $\mu\text{g l}^{-1}$), multiplied by the dilution factor (4) and the electrolyte volume (4 ml), divided by the deposited mass (0.56 μg), and multiplied by 100%.

Results and Discussion

TEM image evaluation.—The differently sized Au NP suspensions were distinct in size, as verified by the TEM images in Fig. 1a.

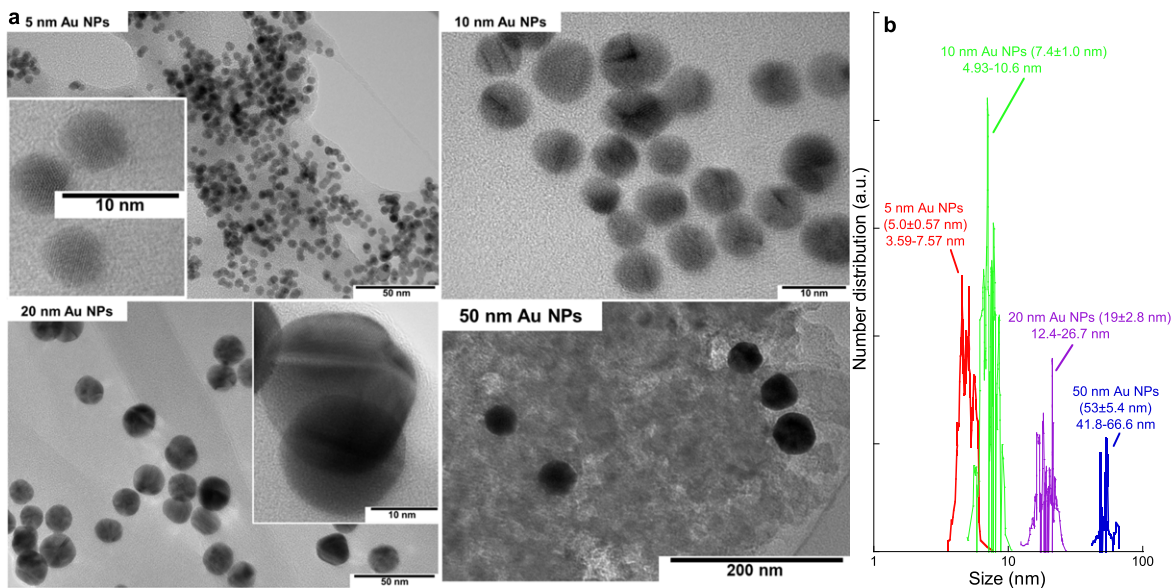


Figure 1. (a) TEM images for the 5, 10, 20, and 50 nm Au NPs at different magnifications and number size distribution based on the TEM image evaluations (129–208 individual particles for each NP suspension), with (b) corresponding mean size, standard deviation, minimum, and maximum size.

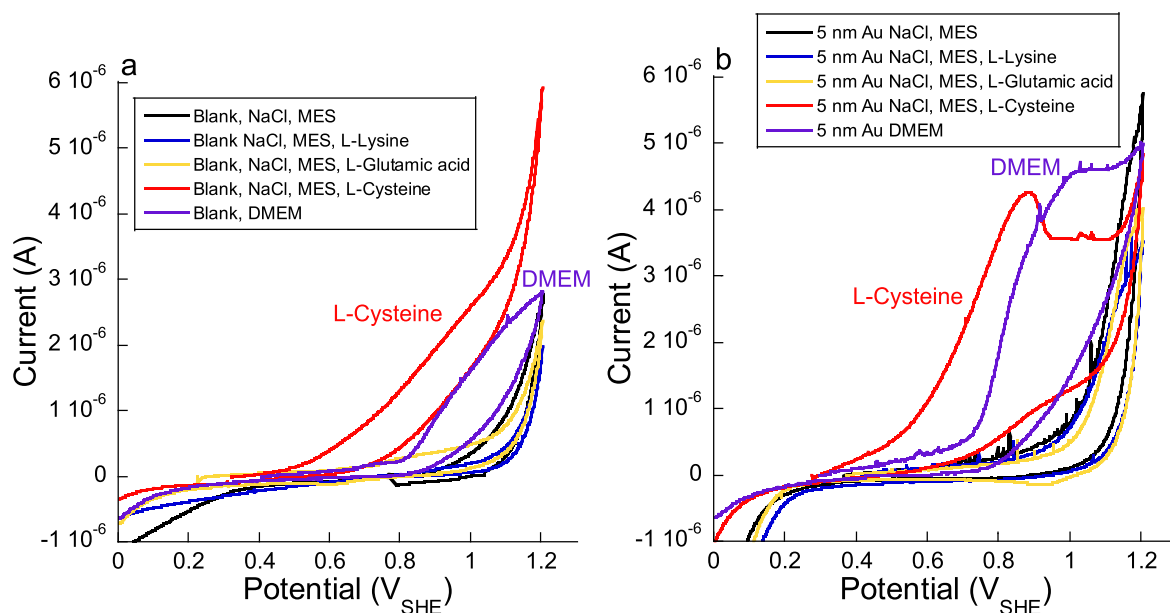


Figure 2. Cyclic voltammograms (Potentiostat 1, PIGE 1) at room temperature, 0.5 mV s^{-1} scan rate, in different electrolytes at pH 7.4, without Au NPs (blank, a) and with $0.56 \mu\text{g}$ deposited 5 nm Au NPs (b). Electrolyte compositions: DMEM; 5 g l^{-1} NaCl, 5 mM MES, 0.5 mM L-Lysine, 0.5 mM L-Glutamic acid, or 0.5 mM L-cysteine. The first cycle is shown in all cases.

The 10 nm Au NPs deviated most from their nominal size (with measured mean value of 7.4 nm), while the 5, 20, and 50 nm Au NPs suspensions complied within 10% of their nominal value (Fig. 1b). However, all four suspensions showed a size distribution which is common for nanoparticles. Except for a small overlap of the size distribution of the 5 and 10 nm Au NP suspensions, all four size distributions were clearly distinct, justifying their use for size-dependent electrochemical studies.

Cyclic voltammetry of differently sized Au NPs immobilized on PIGEs.—Next, it was evaluated whether L-cysteine was a good model amino acid to investigate biomolecule-involved Au oxidation/dissolution processes of relevance for in-vitro and in-vivo conditions. Amino acids of different charges at pH 7.4, and the DMEM cell medium (Table A-I), were compared for the 5 nm Au NPs,

Fig. 2. L-lysine (positively charged at pH 7.4) and L-glutamic acid (negatively charged at pH 7.4) did not reveal any electrochemical activity (with and without Au NPs), while there was a notable oxidation peak induced by DMEM and L-cysteine both in the absence (Fig. 2a) and presence (Fig. 2b) of 5 nm Au NPs. In both cases, the presence of 5 nm Au NPs clearly increased the peak at about 0.85 and 1 V_{SHE} for L-cysteine and DMEM at 0.5 mV s^{-1} scan rate, respectively. DMEM does not contain L-cysteine, but its dimer (cystine) (Table A-I).

L-cysteine interactions with nanoporous Au, Au NP modified electrodes, and Au electrodes have been investigated previously.^{10,11,13} It was found that the Au oxidation and cysteine oxidation peaks overlap. It was further found previously that there was a double peak,¹¹ believed to be assigned to the oxidation of adsorbed cysteine (CySH_{ads}) to cystine (CyS_{ads}), an adsorbed

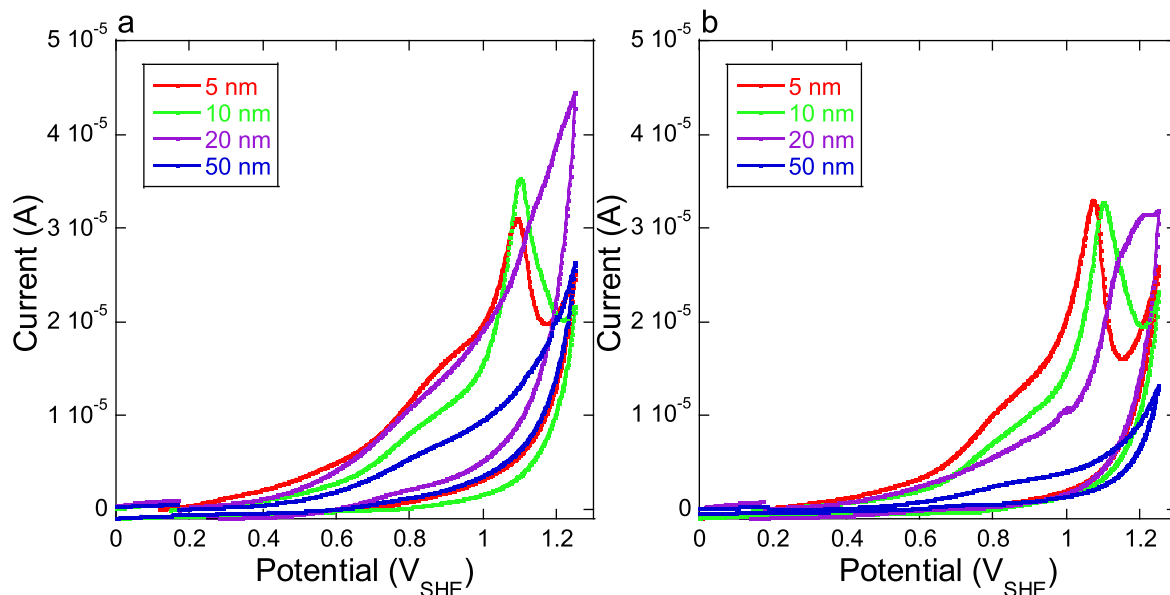


Figure 3. Cyclic voltammograms (Potentiostat 3, PIGE 2) at 24 °C, 5 mV s⁻¹ scan rate, in 5 g l⁻¹ NaCl, 5 mM MES, and 0.5 mM L-cysteine at pH 7.4, with 0.56 μg deposited 5, 10, 20, or 50 nm Au NPs (constant mass: (a)) or 5, 10, 20, and 50 nm Au NPs corresponding to a total deposited Au nominal surface area of 0.086 cm² (constant surface area: (b)). The first cycle is shown in all cases.

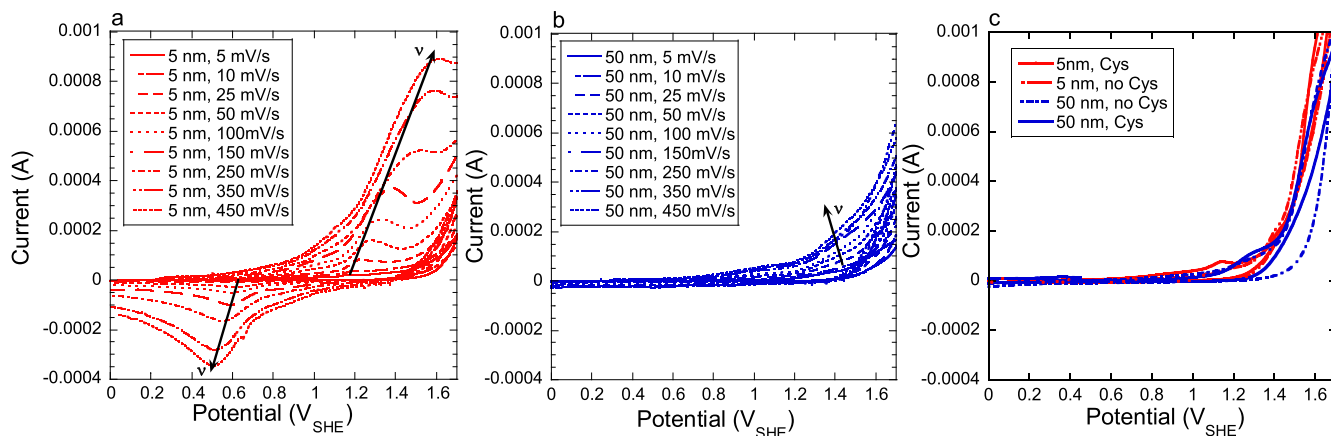
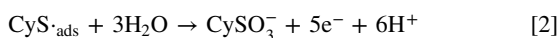
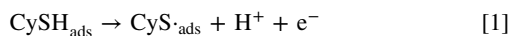


Figure 4. Cyclic voltammograms measured with Potentiostat 1, PIGE 1 at room temperature, at 5–450 mV s⁻¹ scan rate for 5 nm Au NPs (a) and 50 nm Au NPs (b), in 5 g l⁻¹ NaCl, 5 mM MES, and 0.5 mM L-cysteine at pH 7.4, with equal mass of Au NPs (0.56 μg), and (c) Potentiostat 2, PIGE 3 at room temperature, at 20 mV s⁻¹ scan rate, in 5 g l⁻¹ NaCl, 5 mM MES, and either the absence or presence of 0.5 mM L-cysteine, pH 7.4, with particles corresponding to a total deposited Au nominal surface area of 0.086 cm² (constant surface area). The first cycle is shown in all cases.

radical (Eq. 1), and its further oxidation to cysteic acid (Eq. 2),^{11,14–16} respectively. The first transition is a one-electron and the second transition, to cysteic acid, a 5-electron process.



The difference between L-cysteine and DMEM (Fig. 2), which contains 0.20 mM cystine but no cysteine, aligns well with this peak assignment, where the first peak (at about 0.85 V_{SHE} in Fig. 2b) related to the oxidation of cysteine is missing in DMEM, but the second peak related to the oxidation of cystine (at about 1 V_{SHE} in Fig. 2b) is visible. However, it cannot be excluded that its oxidation peak contains contributions from any of the other amino acids, vitamins, and nutrients in DMEM (Table A-D).

The value of the open circuit potential seemed to depend both on the electrolyte composition and on the presence and size of Au NPs. 5 nm Au NPs in the electrolyte containing L-cysteine showed the

lowest open circuit potential (263 ± 56 mV_{SHE}) and a blank PIGE (PIGE 1) in 5 mM MES, 5 g l⁻¹ NaCl, pH 7.4, without any particles, revealed the highest open circuit potential (799 ± 91 mV_{SHE}). The presence of L-cysteine caused for all four sizes of the Au NPs the lowest open circuit potential value, when compared to other amino acids or just the background electrolyte. In the absence of Au NPs, the open circuit potential of the PIGE was also among the lowest (370 ± 30 mV_{SHE}) in the presence of L-cysteine.

Due to the strong oxidation peak of L-cysteine, its lowering effect on the open circuit potential of Au NPs, and its relevance for DMEM, we decided to continue with electrolytes containing L-cysteine.

Figure 3 illustrates the clear size effects of the NPs, independent of whether the deposited mass or the nominal surface area was held constant. With decreased particle size, the cysteine/Au peaks (at about 0.85 and 1.05 V_{SHE}) were clearly more distinct.

The size effect was reproducible among three potentiostats and 3 PIGEs (PIGE 1–3), but not PIGE 4, which showed a higher background current and very weak peaks even for the smallest Au

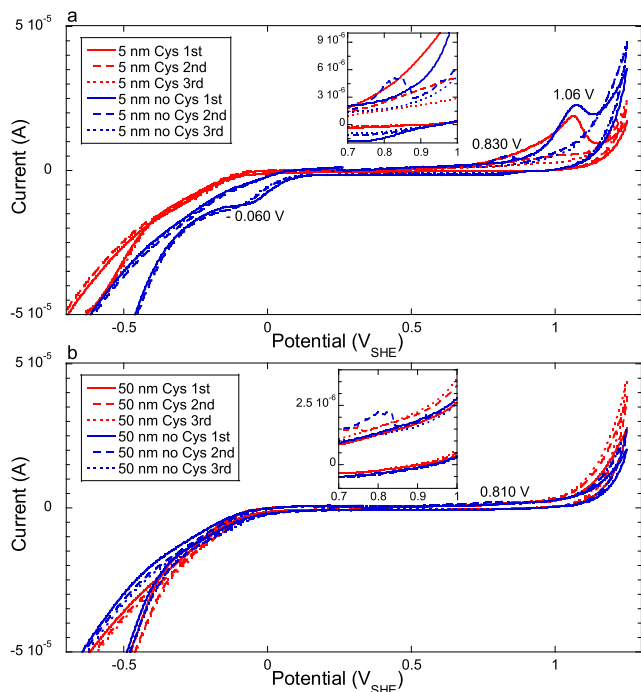


Figure 5. Cyclic voltammograms (Potentiostat 3, PIGE 2) of 5 (a) and 50 (b) nm Au NPs, with particle masses corresponding to a total deposited Au nominal surface area of 0.086 cm^2 (constant surface area), measured for 5 mV s^{-1} scan rate at 24°C for three cycles in 5 g l^{-1} NaCl, 5 mM MES, and the presence or absence of 0.5 mM L-cysteine, at pH 7.4. Insets show the peak around $0.8 \text{ V}_{\text{SHE}}$ at a higher magnification.

NPs (Fig. A-1). Even PIGE 3 showed a higher background current, when compared to PIGE 1–2, and weaker distinct size-dependent peaks (Fig. 4c). However, it was still able to identify a size effect of the Au NPs. Further, we found a difference between potentiostat 1 and potentiostats 2&3 in terms of a higher tendency of current spikes, for example visible in Fig. 2b. Those spikes were hence considered to be artifacts. Figure 4 illustrates the difference between potentiostat 1 (using PIGE 1) and potentiostat 2 (with PIGE 3). Potentiostat 2 produced smoother curves but PIGE 3 revealed a higher background current and weaker peaks. Still, the peak positions and size effect are similar (Fig. 4c) to potentiostat 1/PIGE 1 (Figs. 4a–4b) and potentiostat 3/PIGE 2 (Fig. 3) for similar testing conditions. The influence of the electrode substrate (PIGE) is discussed below.

Effect of scan rate.—Nine scan rates ranging from 5 to 450 mV s^{-1} were tested for the 5 and 50 nm Au NPs (same mass) and it was found that the main peak area, e.g., at $1.2 \text{ V}_{\text{SHE}}$ for 25 mV s^{-1} and 5 nm Au NPs, related to the presence of L-cysteine, is increasing with increasing scan rate, and much larger for the 5 nm Au NPs than for the 50 nm Au NPs for all scan rates, Figs. 4a–4b. Figure 4c shows that this peak is absent when L-cysteine is absent and that 5 nm Au NPs reveal a stronger oxidation peak at lower potential than the 50 nm Au NPs when the same nominal surface area of the particles is compared (much higher mass for the 50 nm Au NPs). Figure A-2 shows the dependence of the peak position and peak area (from Fig. 4) on the scan rate for the 5 nm Au NPs (due to a too weak peak, the 50 nm Au NPs' peaks could not be evaluated). The scan rate affected the peak positions qualitatively in a similar way as reported previously.¹¹ The peak position dependence on the logarithm of the scan rate can be described by two different linear regions, as previously reported,¹¹ Fig. A-2a. Quantitatively, the peak positions were more positive in this work (about 0.1 V) compared to the nanoporous Au electrode reported previously,¹¹ and the slope of the peak positions over the logarithm of the scan rate was more

positive in this work (0.1 compared with 0.06 for the range 5 – 50 mV s^{-1} , 0.37 compared with 0.25 for the range of 100 – 450 mV s^{-1}). This might be caused by a larger resistance of the PIGE substrates with Au NPs as compared to a porous Au electrode. The peak current varied almost linearly with the square root of the scan rate (Fig. A-2b), indicating a partially irreversible reaction,¹⁷ which is also indicated by the shift of the anodic (to positive potentials) and cathodic (to negative potentials) peaks with the logarithm of the scan rate (Figs. 4a and A-2a).

The exact peak position depends on the scan rate, stirring, and type of voltammetry such as stripping voltammetry. For example, the double peak positions of cysteine/Au on the nanoporous Au electrode were at 0.84 and $1.04 \text{ V}_{\text{SHE}}$ at a 50 mV s^{-1} scan rate with rotation rates of 300 to 3000 rounds per minute in a previous study,¹¹ which is very similar to reported cyclic voltammograms of Au NP modified glassy carbon electrodes in the presence of cysteine,¹⁰ to cysteine oxidation peaks on an Au electrode,¹³ and to the present work for 5 and 10 nm Au NPs at 5 mV s^{-1} scan rate (Fig. 3).

The peak area, which is proportional to the peak height, was roughly linearly dependent on the square root of the scan rate, indicating a diffusion-controlled process, Fig. A-2b, in agreement with previous work using a nanoporous electrode.¹¹

Stability of Au NPs during cycling.—Figure 5 shows three full cycles of 5 and 50 nm Au NPs (same nominal surface area) in the presence and absence of L-cysteine at 5 mV s^{-1} scan rate. L-cysteine results in a broad peak for the first cycle of 5 nm Au NPs with a main peak position at around $1.06 \text{ V}_{\text{SHE}}$. The broad peak suggests that this peak corresponds to at least two different oxidation processes. The main peak at $1.06 \text{ V}_{\text{SHE}}$ has a smaller area due to a different baseline than in the absence of L-cysteine. In the absence of L-cysteine, the Au oxidation peak (at $1.06 \text{ V}_{\text{SHE}}$) corresponds to what would be expected for the oxidation of Au^0 to $\text{Au}(\text{OH})_3$ or to AuCl_4^- .^{7,8,18}

While there is no significant difference between the presence and absence of L-cysteine for the reduction curve for the 50 nm Au NPs (Fig. 5b), there is a clear difference for the 5 nm Au NPs (Fig. 5a), with a reduction peak at $-0.06 \text{ V}_{\text{SHE}}$ only in the absence of L-cysteine. This indicates that the formed oxidized species on the Au NPs ($\text{Au}(\text{OH})_3$ or surface-adsorbed AuCl_4^-) in the absence of L-cysteine is reduced back, but this reduction is hindered in the presence of L-cysteine. Also, a clearly shifted hydrogen evolution curve towards more negative potentials can be observed in the presence of L-cysteine for the 5 nm Au NPs, which also indicates that L-cysteine is irreversibly (no reduction peak) interacting with the surface of the 5 nm Au NPs, but not the 50 nm Au NPs.

The second cycle results in an oxidation peak at around $0.8 \text{ V}_{\text{SHE}}$ for the 5 nm Au NPs, and to a smaller extent for the 50 nm Au NPs, but only in the absence of L-cysteine. This peak is much smaller than the Au oxidation peak at $1.06 \text{ V}_{\text{SHE}}$ in the first cycle. As the electrolyte does not contain L-cysteine, this peak is most probably related to a Au species oxidation, although it is unclear which and why it is shifted.

Most interestingly, all Au oxidation peaks seem to disappear after only three cycles for the 5 nm Au NPs. Figure A-3 shows two full cycles of an Au foil in the presence and absence of L-cysteine, for comparison. There was no clear trend with increasing or decreasing peaks upon cycling, which suggests that the peak disappearance for the Au NPs is caused by either detachment from the PIGE, a mass limitation, or irreversible oxidation. As for the Au NPs, the Au foil oxidation peak at 1.2 – $1.5 \text{ V}_{\text{SHE}}$ (20 mV s^{-1} scan rate) was larger in the presence of L-cysteine. As for the 5 nm Au NPs, a reduction peak at $-0.35 \text{ V}_{\text{SHE}}$ was only visible in the absence of L-cysteine. The hydrogen evolution peak was shifted towards more positive potentials in the presence of L-cysteine for the Au foil—the opposite trend as for the 5 nm Au NPs.

To further investigate any oxidation/detachment of the Au into solution, inductively coupled plasma secondary ion mass spectrometry was used to quantify any dissolved/detached Au, after 5 and 50 nm drop-casted Au NPs had been cycled 10 times at 450 mV s^{-1} ,

in an electrolyte containing L-cysteine. The amount of Au in solution corresponded to 6 and 17% of the initially deposited mass of the 50 and 5 nm Au NPs, respectively. One needs to be careful to not over-interpret these numbers, as they just represent one experiment and may contain both dissolved species and detached Au NPs. The separation of 5 nm Au NPs from dissolved Au species, which are easily precipitating as Au⁰ in dilute solutions and solutions not containing aqua regia, is challenging, but can be achieved in future studies with certain filtering or combined flocculation/centrifugation methods for similar 5 nm Au NPs as in this work.^{4,5} It is, however, clear that Au was detected in the electrolyte in this work.

The oxidation peak at 1.06 V_{SHE} in Fig. 5a in the absence of L-cysteine, believed to correspond to Au oxidation, was further evaluated by means of Faraday's law, assuming a three-electron transition. In the absence of L-cysteine, Au⁰ could either oxidize to Au(OH)₃ or to AuCl₄⁻,⁷ both of which would be a three-electron transition process. The peak area (7.06 10⁻⁷ A·V) was evaluated in Origin 2016 and converted to charge by multiplying by 0.005 V s⁻¹ (the scan rate). The charge was multiplied by the molar mass of Au, divided by Faraday's constant and 3 (the number of transferred electrons), resulting in 0.096 μg, which corresponds to 69% of the deposited 5 nm Au mass for this experiment. This would indicate that most of the 5 nm Au NPs oxidize during that first cycle.

Aqueous Au released from bulk Au in a one-month immersion experiment in different amino acids revealed that L-cysteine was able to dissolve Au.⁶ In the present work, we did not detect any similarly sized, or even any, reduction peak related to L-cysteine or Au reduction in the presence of L-cysteine (see Figs. 5 and A.3). It remains to be investigated whether oxidation of Au in the presence of L-cysteine, or oxidation of L-cysteine in the presence of Au NPs, is irreversible or results in the release of aqueous species into solution, or both.

Effect of NP size and L-cysteine.—This study found consistently stronger oxidation peaks for smaller (5 and 10 nm) Au NPs, while 20 and 50 nm Au NPs showed minor or no peaks under similar experimental conditions. This finding is expected for a similar mass, as smaller particles have a larger specific surface area. However, it was also found for a similar nominal surface area.

If smaller NPs agglomerate more, and the current signal is greater than for larger NPs for the same nominal surface area, then the effect that leads to an increased current has to be even more significant than observed in the experiments. Hence, in this work, we found a clear size effect despite possible agglomeration.

A recent study electrochemically investigated nine different citrate-coated Au NP size fractions ranging from about 30 to 120 nm in the presence of L-cysteine.¹⁹ While the reference electrode has not been described in that study,¹⁹ it generally agreed with the present work in the sense that larger Au NPs oxidized at higher potential and with smaller oxidation peak areas. Also, the first L-cysteine oxidation peak (denoted "electrochemical catalytic oxidation of cysteine" in that study¹⁹) shifted towards more positive potentials and decreased in area for larger Au NP sizes, which is also in agreement with the present work. Another study on 4–250 nm Au NPs chemisorbed on a glassy carbon/indium-tin oxide electrode came to a similar conclusion with more positive Au oxidation potentials for larger sized Au NPs.²⁰ The same group also found this effect for silver NPs.²¹ They suggested that diffusion alone could not explain this phenomenon, but that different surface energies for differently sized NPs would result in different redox potentials.^{20,21} This has been theoretically predicted previously.²²

There are several possible explanations for the strong size effect found in this work and in another study on larger NPs.¹⁹ First, the cyclic voltammograms in this work were measured in stagnant solutions, which means that the diffusion layer thickness is time-dependent. Changes of the pH-value, however, have a strong influence on the electrochemical signal. Some of the authors of

this study have shown in simulations that the pH-gradients are steeper (and closer to the NP surface) for smaller nanoparticles.²³ These differences to planar surfaces become significant for nanoparticle sizes <10 nm. Second, time-of-flight secondary ion mass spectrometry measurements performed on the 5 and 50 nm Au NPs of this study showed a strong interaction between the 5 nm Au NPs and cysteine,⁹ forming an Au thiolate complex. It might be possible that complexation is facilitated by a smaller NP size. This has been suggested for thiol complexes with silver NPs.²⁴

Note that all these possible underlying reasons for the size effect—different pH gradient, altered diffusion, different surface energies, varying strength and ability to form surface complexes with cysteine (an electroactive compound)—would increase the anodic peaks related to either Au or cysteine oxidation with decreasing Au NP size.

Facilitated oxidation and formation of an Au thiolate complex with decreased NP size is interesting from a corrosion and hazard assessment perspective, as amino acids, including cysteine, are present in the human body along with strongly oxidizing potentials, such as under inflammatory conditions, e.g. induced by macrophages. The findings of this study are relevant for, and could assist in understanding, the "unexpected" dissolution^{3–5} of very small (<10 nm) Au NPs in-vivo.

Influence of electrodes and limitations of this study.—The drop casting method applied in this study is a frequently used method for the preparation of reactive electrode surfaces. An unintended phenomenon of this technique is the so-called "coffee ring effect": After the drop cast and drying of the colloidal suspension, the NPs are not deposited evenly on the surface, leaving the center of the electrode surface with a lower particle density.^{25,26} Larger agglomerates of NPs might also detach by means of forces caused by gravity or flows. While the present study detected Au in solution after electrochemical cycling, it remains unclear whether aqueous Au was comprised of detached Au NPs or oxidized/complexed Au species. The reproducibility of the drop casting method in the present study was not investigated specifically, but it was found that the variability among PIGEs was far greater than among individual drop casting procedures, independent of the operator.

PIGE 4 had such a high background current and showed peaks that were so weak that this PIGE could not be used to distinguish the Au NP size effect at all. PIGE 3 showed higher background current and weaker peaks but could still reproduce the same general trends as PIGE 1 and PIGE 2. PIGE 2 was the most sensitive electrode and the only electrode, which showed a clear oxidation peak of 5 nm Au NPs in the absence of L-cysteine. It is likely that the resistance and/or impurity level of the electrodes differed, as well as the conductivity between the deposited Au NPs and the electrode. This is determined by the purity of the graphite rod and the fraction of paraffin to graphite. While these differences may not matter for higher masses or more reactive particles, they become highly relevant for low masses of Au NPs, as investigated in this study. Similar variations were previously found for different glassy carbon electrodes used for trace metal analysis.²⁷

Conclusions

Electrochemical measurements of drop casted Au NP suspensions on graphite electrodes are susceptible to the quality of the electrode, detachment into solution, and pre-treatments (cycling, pre-immersion) of the Au NPs. While we found considerable variations in the suitability of different graphite-based electrodes to sense size differences of drop-casted Au NPs in an electrolyte containing L-cysteine at pH 7.4, general conclusions were reproduced by three potentiostats, three electrodes, and three labs. Smaller sized (5, 10 nm) Au NPs were significantly more susceptible to electrochemical L-cysteine interactions and/or L-cysteine-facilitated Au

oxidation than larger (20, 50 nm) sized nanoparticles, both for the same mass and nominal surface area of Au NPs. Au oxidation seems to be facilitated by the presence of L-cysteine and a smaller particle size.

Acknowledgments

We would like to acknowledge funding from the Swedish Foundation for Strategic Research (SSF, #FFL18-0173), the Swedish Research Council (VR, #2019-03657), from the Swedish Steel Producer's Association Jernkontoret (Stiftelsen Skandinaviska Malm 6–2020), the European Union Program MOST (#R-QSUA-65035), the Ministry of Science and Higher Education of the Russian

Federation in the framework of Increase Competitiveness Program of NUST «MISiS» (grant number K2-2020-024), implemented by a governmental decree dated 16th of March 2013, N 211, the Wolfe-Western fellowship, Canada (#2020), the Canada Research Chairs Program (#950-233099), startup funds at Western University, Canada (Dept. Chemistry, 2020), co-funding from BioTalent Canada for a Western Science internship, and funding from the New Frontiers in Research Fund, Transformation, Canada (#NFRFT-2020-00573).

Appendix

Table A-I. Composition of DMEM.

Component	mg l ⁻¹	mM
Glycine	30	0.4
L-arginine hydrochloride	84	0.40
L-cystine 2HCl	63	0.20
L-glutamine	584	4.0
L-histidine hydrochloride-H ₂ O	42	0.20
L-isoleucine	105	0.80
L-leucine	105	0.80
L-lysine hydrochloride	146	0.80
L-methionine	30	0.20
L-phenylalanine	66	0.40
L-serine	42	0.40
L-threonine	95	0.80
L-tryptophan	16	0.078
L-tyrosine disodium salt dehydrate	104	0.40
L-valine	94	0.80
Choline chloride	4.0	0.029
D-calcium pantothenate	4.0	0.0084
Folic acid	4.0	0.0091
Niacinamide	4.0	0.033
Pyridoxine hydrochloride	4.0	0.019
Riboflavin	0.4	0.0011
Thiamine hydrochloride	4.0	0.012
i-inositol	7.2	0.040
Calcium chloride (CaCl ₂) (anhyd.)	200	1.8
Ferric nitrate (Fe(NO ₃) ₃ ·9H ₂ O)	0.10	0.00025
Magnesium sulfate (MgSO ₄) (anhyd.)	98	0.81
Potassium chloride (KCl)	400	5.3
Sodium bicarbonate (NaHCO ₃)	3700	44
Sodium chloride (NaCl)	6400	110
Sodium phosphate monobasic (NaH ₂ PO ₄ ·H ₂ O)	125	0.91
D-glucose (dextrose)	4500	25
Phenol red	15	0.040

Table A-II. Overview on combinations of potentiostats and electrodes used in the present study.

Potentiostat	Electrode	Tested conditions
Potentiostat 1	PIGE 1	Different amino acids, control solutions, NP sizes, scan rates (Figs. 2, 4a, 4b, A-1, A-2)
Potentiostat 2	PIGE 3, PIGE 4, Au foil	Different NP sizes, cysteine presence/absence, scan rates (Figs. 4c, A-1, A-3)
Potentiostat 3	PIGE 2	Different NP sizes, cycling (Figs. 3, 5)

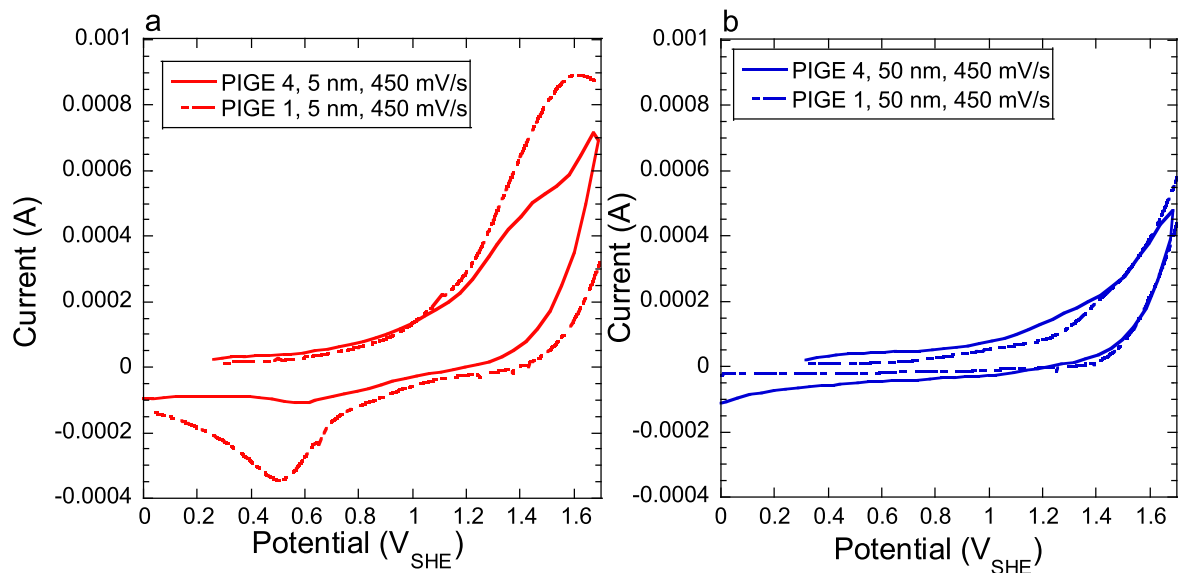


Figure A.1. Cyclic voltammograms of 5 nm NPs (a) and 50 nm NPs (b) with Potentiostat 2 and PIGE 4 (solid lines) and Potentiostat 1 and PIGE 1 (dashed lines), measured for 450 mV s⁻¹ scan rate at 25 °C in 5 g l⁻¹ NaCl, 5 mM MES, and 0.5 mM L-cysteine, at pH 7.4.

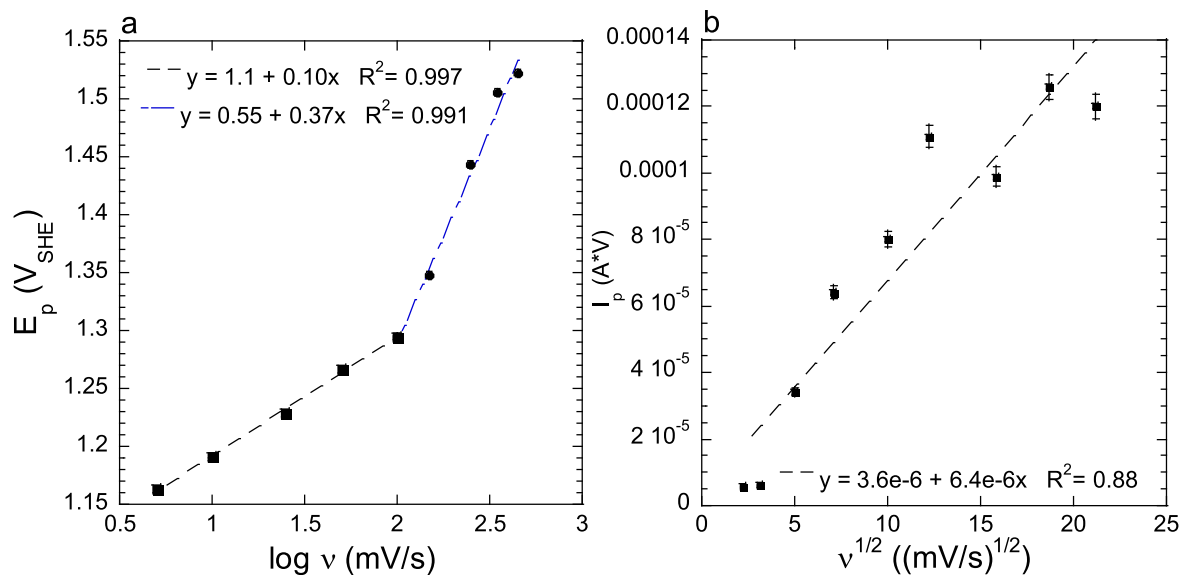


Figure A.2. Anodic peak positions (a) and peak areas (b) from Fig. 4a (5–450 mV s⁻¹ scan rate for 5 nm Au NPs, room temperature, Potentiostat 1, PIGE 1, 5 g l⁻¹ NaCl, 5 mM MES, and 0.5 mM L-cysteine at pH 7.4) as a function of the scan rate ν, log ν (a) and the square root of ν (b). Peak areas were determined at the peak positions indicated in (a) and using a linear baseline. Linear trendlines are shown as dashed lines.

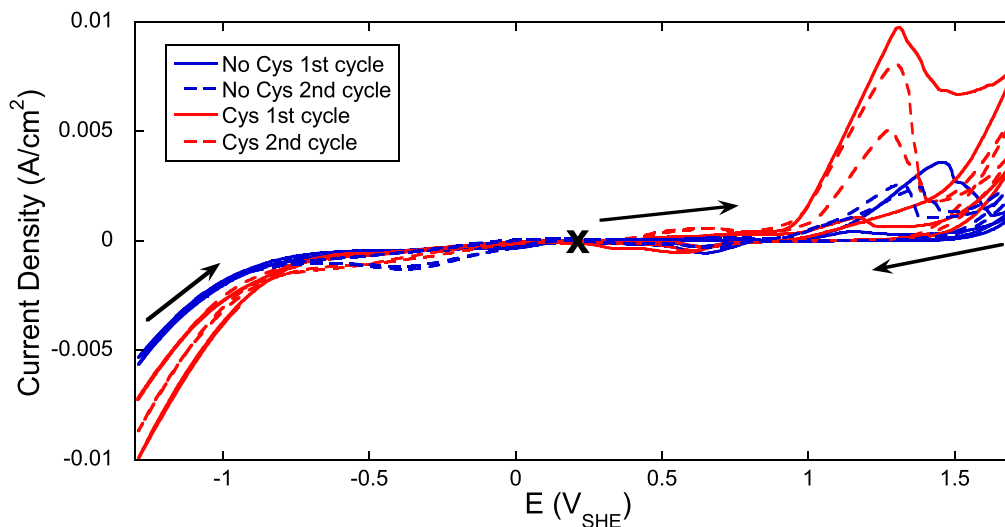


Figure A-3. Cyclic voltammograms (Potentiostat 2) of a Au foil, measured for 20 mV s^{-1} scan rate at $25 \text{ }^\circ\text{C}$ for two cycles and two replicate measurements in 5 g l^{-1} NaCl, 5 mM MES, and the presence or absence of 0.5 mM L-cysteine, at pH 7.4. Note that the second cycle either is showing a larger or smaller oxidation peak for different replicate measurements (in both electrolytes), which suggests different initial surface conditions. The measurement order was replicate 1 and 2 in the absence of L-cysteine, followed by replicate 1 and 2 in the presence of L-cysteine. The Au foil was cleaned (not repolished) prior to each measurement. “x” denotes the approximate start at open circuit potential ($0.1\text{--}0.3 \text{ V}_{\text{SHE}}$) and the arrows show the direction of the scan (oxidation, reduction, oxidation).

ORCID

Yolanda S. Hedberg  <https://orcid.org/0000-0003-2145-3650>

References

- J. Zhang, L. Mou, and X. Jiang, *Chem. Sci.*, **11**, 923 (2020).
- N. S. Abadeer and C. J. Murphy, *J. Phys. Chem. C*, **120**, 4691 (2016).
- A. Balfourier, N. Luciani, G. Wang, G. Lelong, O. Ersen, A. Khelifa, D. Alloyeau, F. Gazeau, and F. Carn, *Proc. Natl Acad. Sci.*, **117**, 103 (2020).
- U. Carlander, K. Midander, Y. S. Hedberg, G. Johanson, M. Bottai, and H. L. Karlsson, *ACS Appl. Bio Mater.*, **2**, 1006 (2019).
- S. McCarrick, K. Midander, M. Krausova, U. Carlander, and H. L. Karlsson, *Int. J. Nanomed.*, **16**, 5895 (2021).
- D. H. Brown, W. E. Smith, P. Fox, and R. D. Sturrock, *Inorg. Chim. Acta*, **67**, 27 (1982).
- N. Finkelstein and R. D. Hancock, *Gold Bull.*, **7**, 72 (1974).
- C. C. Nesbitt, E. B. Milosavljevic, and J. L. Hendrix, *Ind. Eng. Chem. Res.*, **29**, 1696 (1990).
- H.-Y. Nie, E. Romanovskaia, V. Romanovski, J. Hedberg, and Y. S. Hedberg, *Biointerphases*, **16**, 021005 (2021).
- M. K. Dey, S. Kumar, and A. K. Satpati, *J. Electroanal. Chem.*, **807**, 119 (2017).
- Z. Liu, H. Zhang, S. Hou, and H. Ma, *Microchim. Acta*, **177**, 427 (2012).
- F. Scholz and B. Lange, *Trends in Analytical Chemistry*, **11**, 359 (1992).
- W. R. Fawcett, M. Fedurco, Z. Kováčová, and Z. Borkowska, *J. Electroanal. Chem.*, **368**, 265 (1994).
- J. Koryta and J. Pradáč, *J. Electroanal. Chem. Interf. Electrochem.*, **17**, 177 (1968).
- J. Koryta and J. Pradáč, *J. Electroanal. Chem. Interf. Electrochem.*, **17**, 185 (1968).
- A. Tudos, P. Vandeberg, and D. Johnson, *Anal. Chem.*, **67**, 552 (1995).
- E. Laviron and L. Roullier, *J. Electroanal. Chem. Interf. Electrochem.*, **115**, 65 (1980).
- H. Nishi and T. Tatsuma, *Angew. Chem. Int. Ed.*, **55**, 10771 (2016).
- P. Cao, N. Wang, D. Chen, S. Sun, H. Ma, and M. Lin, *Gold Bull.*, **54**, 97 (2021).
- O. S. Ivanova and F. P. Zamborini, *Anal. Chem.*, **82**, 5844 (2010).
- O. S. Ivanova and F. P. Zamborini, *J. Am. Chem. Soc.*, **132**, 70 (2010).
- W. Plieth, *J. Phys. Chem.*, **86**, 3166 (1982).
- T. Stepan, L. Tété, L. Laundry-Mottiar, E. Romanovskaia, Y. S. Hedberg, H. Danninger, and M. Auinger, *Electrochim. Acta*, 139923 (2022).
- A. Henglein, *J. Phys. Chem.*, **97**, 5457 (1993).
- Y. Ooi, I. Hanasaki, D. Mizumura, and Y. Matsuda, *Sci. Technol. Adv. Mater.*, **18**, 316 (2017).
- A. K. S. Kumar, Y. Zhang, D. Li, and R. G. Compton, *Electrochem. Commun.*, **121**, 106867 (2020).
- T. A. Lowe, J. Hedberg, M. Lundin, S. Wold, and I. O. Wallinder, *Int. J. Electrochem. Sci.*, **8**, 3851 (2013).